

INITIAL GEOMETRIC UNCERTAINTY ASSESSMENT IN COMPRESSOR AIRFOILS USING PHYSICS-BASED DIRECT MANIPULATED FFD

Kotaro OMOTO[1], Daisuke SASAKI[1], Kotaro MATSUI[2] & Mai YAMAGAMI[2]

[1]Osaka Metropolitan University, Sakai, Japan
[2]IHI Corporation, Akishima, Japan

Abstract

Jet engines must reduce their fuel consumption to meet recent societal demands. Because a high pressure ratio and high bypass ratio are needed for reducing fuel consumption, recent jet engines tend to be 'small-core'. One aspect of a small core is that the influence of dimensional tolerance is relatively large. Therefore, it is necessary to develop a design method for robustness against small cores by considering geometric uncertainty. In this study, the effect of geometric uncertainty on compressor rotor blades for jet engines was investigated using a 2D CFD. Geometric uncertainty is represented using the PBDMFFD method, and three types of airfoils with different LE shapes are used as baseline geometries. The deformation is applied only near the LE, and the direction of the deformation is set to be normal to the chord line to change the metal angle. First, to validate the CFD analysis, the CFD results of the nominal airfoils are compared with experimental results, and a qualitative agreement is observed in the characteristics of performance due to differences in LE shapes and sensitivity to incidence angles. Next, deformations are applied to each airfoil, and the analysis of the changes in performance caused by the geometric uncertainty is conducted. The results are organized by the normalized loss coefficient, and it is shown that the variance of the performance due to geometric uncertainty differs depending on the baseline airfoil. In terms of the maximum value and variance, the values differ significantly for each airfoil, while in terms of the minimum value, the values are approximately the same for all airfoils. These results are important for understanding the relationship between the LE geometry and performance, and they provide insights for future robust optimal design.

Keywords: CFD, Geometric-Deformation, Uncertainty, Compressor

1. Introduction

The global initiative toward a sustainable society, as outlined in the Sustainable Development Goals of the United Nations, has intensified the demand for carbon-neutral solutions in all industries. In aeronautical engineering, research on sustainable aviation fuels is being conducted to achieve a carbon neutral society. Simultaneously, a reduction in fuel burn is essential. To reduce fuel burn, the weight and specific fuel consumption (SFC) must be reduced.

To achieve a lower SFC, modern jet engines are inclined toward higher bypass ratios (BPR) and higher overall pressure ratios (OPR). According to Kato et al. [1], increasing the BPR and OPR resulted in a lower final-stage blade height. The physical size of the final stage is indicated by the corrected flow rate of the compressor outlet, and it is used to determine the core size. With high BPR and OPR, the turbofan engine tends to have a small core. A critical challenge with these downsized components is that their performance becomes more sensitive to manufacturing tolerances, where small geometric deviations can lead to performance degradation [2]. This requires the integration of a geometric uncertainty analysis into the design process [3].

In a previous study, we simulated geometric uncertainty by applying global disturbances to the entire airfoil to evaluate performance variability [4]. This study identified a strong correlation between

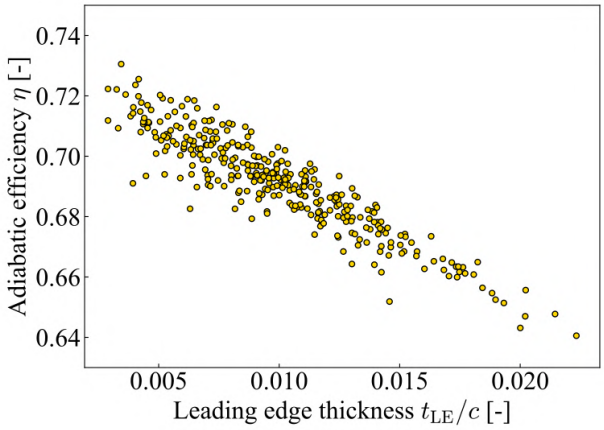


Figure 1 – Relationships between the LE thickness and the adiabatic efficiency [4].

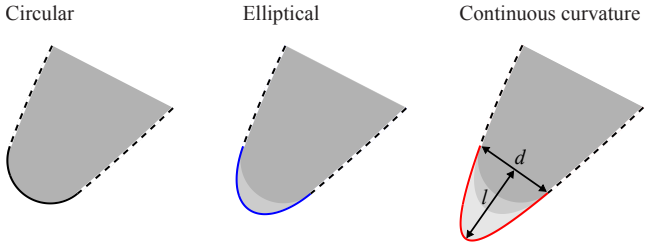
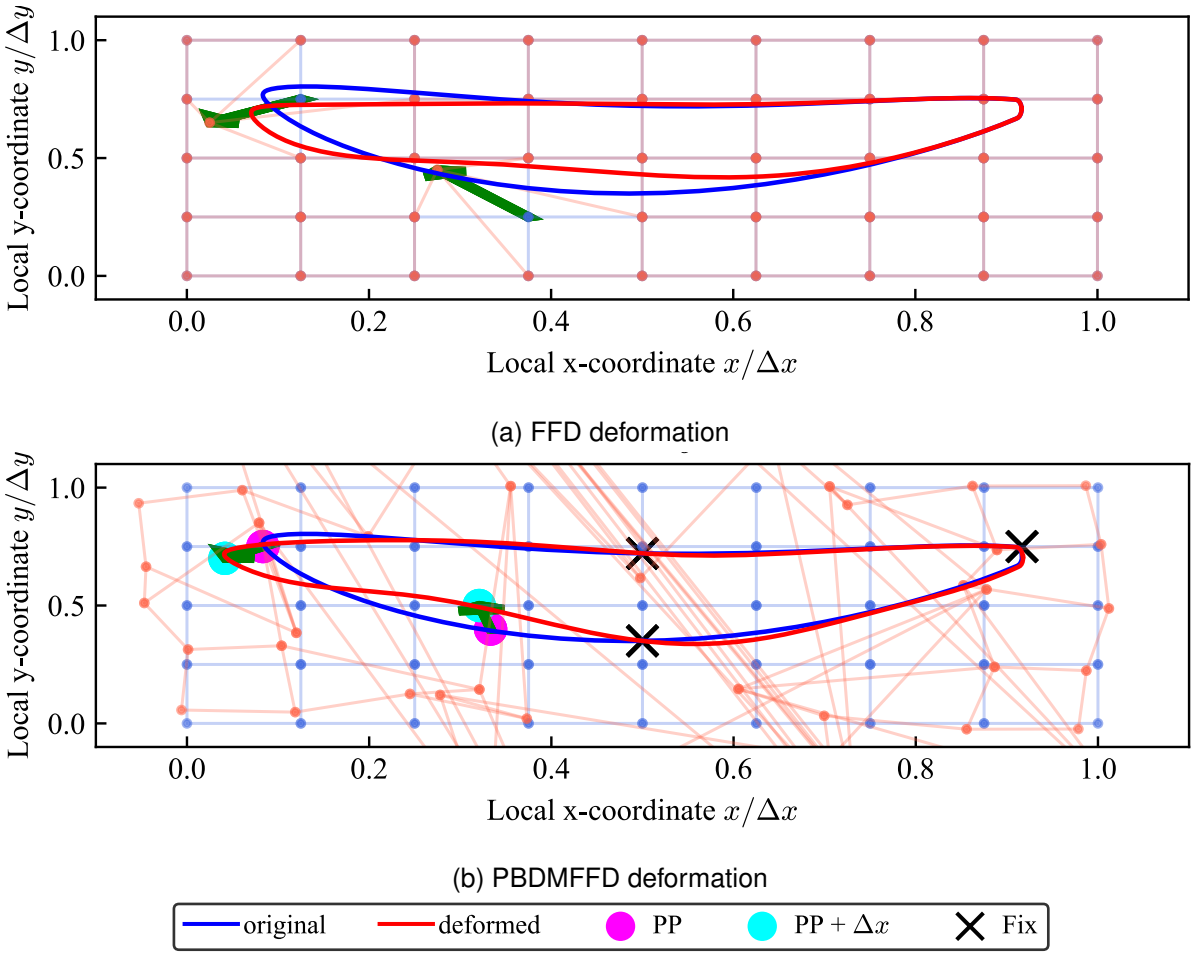


Figure 2 – Baseline airfoils for CFD analysis [6].

the leading-edge (LE) thickness (a geometric parameter) and the adiabatic efficiency (a performance parameter), as shown in Figure 1. Although this method is efficient and effective in applying manufacturing variation to the entire blade, it is not suitable for representing local uncertainties confined to the LE region or geometric uncertainties involving changes in the metal angle. To address these limitations, the Physics-Based Direct Manipulated Free-Form Deformation (PBDMFFD) method proposed by Yamazaki et al. [5] is introduced. Conventional Free-Form Deformation (FFD) method deforms a shape by controlling points of a control box; while defining the deformation is straightforward, the calculation lacks physical meaning, often resulting in non-intuitive deformed shapes. On the contrary, PBDMFFD extends conventional FFD by incorporating physical significance into the deformation process. Furthermore, it allows for the control of Pilot Points (PP), offering the advantage of generating intuitive deformed shapes.

Against this background, the objective of this study is to evaluate the variation in compressor airfoil performance caused by local geometric uncertainty and to obtain insights for the final goal of establishing a robust design system for compressor blades that can account for manufacturing uncertainty. Local geometric uncertainty is applied using PBDMFFD, and steady-state, 2D Computational Fluid Dynamics (CFD) is performed using Ansys CFX. Three airfoils shown in Figure 2, whose performance characteristics were experimentally evaluated by Lang et al. [6], were selected as baseline geometries: one with a circular LE (Circular), one with a continuous curvature LE (Continuous Curvature) , and one with a elliptical LE (Elliptical). For these three airfoils with distinct LE geometries, manufacturing variations are simulated by altering the shape near the LE. Equivalent variations are applied to all baselines to analyze how performance variability differs between the three geometries, thereby evaluating the characteristics of each airfoil with respect to manufacturing geometric uncertainty. The final goal is to quantify the uncertainty through these CFD analyses, which clarifies the impact of geometric uncertainty on the performance of the compressor airfoil.



(a) FFD deformation

(b) PBDMFFD deformation

Figure 3 – Example of FFD deformation and PBDMFFD deformation.

2. Methodology

2.1 PBDMFFD

In this study the PBDMFFD method is used to apply local geometric uncertainty to the baseline airfoils. The PBDMFFD was introduced by Yamazaki et al. [5] and is an extension of the conventional FFD method. The conventional FFD and PBDMFFD methods deform a shape by using a control box, which covers the shape to be deformed shown in Figure 3. The difference between the two methods is the definition of the control points. Equation (1) is the foundational equation of the FFD method,

$$\Delta \mathbf{x} = \mathbf{B} \cdot \Delta \mathbf{P}, \tag{1}$$

where $\Delta \mathbf{x}$ is the displacement of the shape or Pilot Points (PP), $\mathbf{B}$ is the blending function, and $\Delta \mathbf{P}$ is the displacement of the control points.

In the conventional FFD method, $\Delta \mathbf{P}$ is firstly defined as a design variable. Then, the displacement of the shape $\Delta \mathbf{x}$ is calculated using Equation (1). Figure 3a shows an example of the deformed airfoil using the FFD method. Two control points are defined near the LE and the suction side of the airfoil. This method is straightforward and easy to calculate, but the deformed shape has no physical meaning, and it is difficult to represent the intended deformed shape.

On the other hand, in the PBDMFFD method, $\Delta \mathbf{x}$ is the displacement of the shape and PP, and it is the design value. First, the displacement of PP is defined, and the displacement of the control points $\Delta \mathbf{P}$ is calculated by using Equation (1). To determine $\Delta \mathbf{P}$, the deformation energy w is introduced as Equation (2):

$$w = \frac{1}{2} \int_{\Theta} \left[\lambda \left(\varepsilon_1 + \varepsilon_2 + \varepsilon_3 \right)^2 + 2\mu \left(\varepsilon_1^2 + \varepsilon_2^2 + \varepsilon_3^2 + 2 \left(\varepsilon_4^2 + \varepsilon_5^2 + \varepsilon_6^2 \right) \right) \right] dQ, \tag{2}$$

where λ and μ are the Lamé's constants. In this study, the Poisson's ratio was set to $\nu = 0.3$. The displacement of control points $\Delta \mathbf{P}$ is determined with the minimization of the deformation energy w.

The calculation of $\Delta\mathbf{P}$ for all control points is completed, then the displacement of the shape $\Delta\mathbf{x}$, which includes the displacement of PP, is re-calculated using the calculated $\Delta\mathbf{P}$ and Equation (1). Figure 3b shows an example of the deformation with the PBDMFFD method. Two PP are set to near the LE and the suction side of the airfoil and three fixed points are set to TE and the mid-chord of the airfoil. While this method needs more calculation cost than the conventional FFD method, the desired deformation can easily be achieved and the deformed shape has physical meaning. Therefore, the PBDMFFD method is suitable of this study, which apply local deformation in the intended direction to the airfoil. In this study the damping function is introduced to avoid discontinuities at the boundary of the control box. The damping function is defined as Equation (3),

$$f(s) = \begin{cases} 0 & \text{if } s \leq s_{\text{start}} \\ \sin\left(\frac{\pi}{2}\frac{s-s_{\text{start}}}{\Delta_{\text{up}}}\right) & \text{if } s_{\text{start}} < s < s_{\text{start}} + \Delta_{\text{up}} \\ 1 & \text{if } s_{\text{start}} + \Delta_{\text{up}} \leq s \leq s_{\text{end}} - \Delta_{\text{down}} \\ \sin\left(\pi + \frac{\pi}{2}\frac{s-s_{\text{end}}}{\Delta_{\text{down}}}\right) & \text{if } s_{\text{end}} - \Delta_{\text{down}} < s < s_{\text{end}} \\ 0 & \text{if } s_{\text{end}} \leq s \end{cases}, \tag{3}$$

where s is the local coordinate of the control box. In this study, each parameter of the damping function is set as follows: $s_{\text{start}} = 0.1$, $s_{\text{end}} = 1$, $\Delta_{\text{up}} = 0.02$, and $\Delta_{\text{down}} = 0.01$. The detail of the PBDMFFD method is described in the original paper by Yamazaki et al. [5].

2.2 CFD Setup

The commercial CFD software Ansys CFX is used for the flow analysis. The simulations solved the Reynolds averaged Navier-Stokes equations for a compressible ideal gas by using the shear stress transport turbulence model. The computational domain is shown in Figure 4. To reduce the computational cost, the flow through the cascade assumed periodic and mid span flow was modeled as a 2D flow, therefore, the computational domain was set to a single pitch and 2D domain. The inlet boundary condition was set as a Mach number of 0.7 and a total temperature of 319 K. The flow angle at inlet and the static pressure at the outlet was specified by the experimental results. The initial condition was set as a nominal results of each airfoil, and the convergence was determined by the stabilization of the loss coefficient, the performance parameter of the compressor airfoils. The loss coefficient ω was calculated with upstream total pressure and static pressure, and downstream total pressure,

$$\omega = \frac{p_{\text{t},1} - p_{\text{t},2}}{p_{\text{t},1} - p_{\text{s},1}}, \tag{4}$$

where $p_{\text{t},1}$ is the total pressure at upstream, $p_{\text{t},2}$ is the total pressure at downstream, and $p_{\text{s},1}$ is the static pressure at upstream.

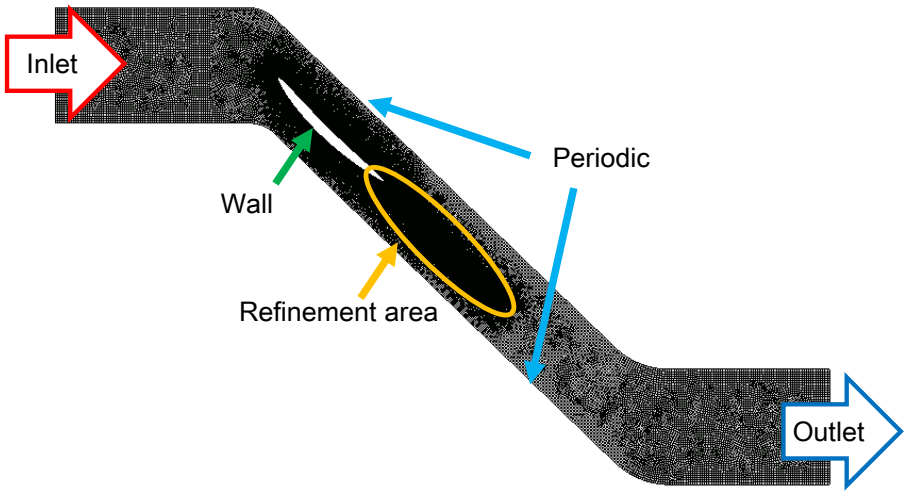


Figure 4 – Computational domain for CFD analysis

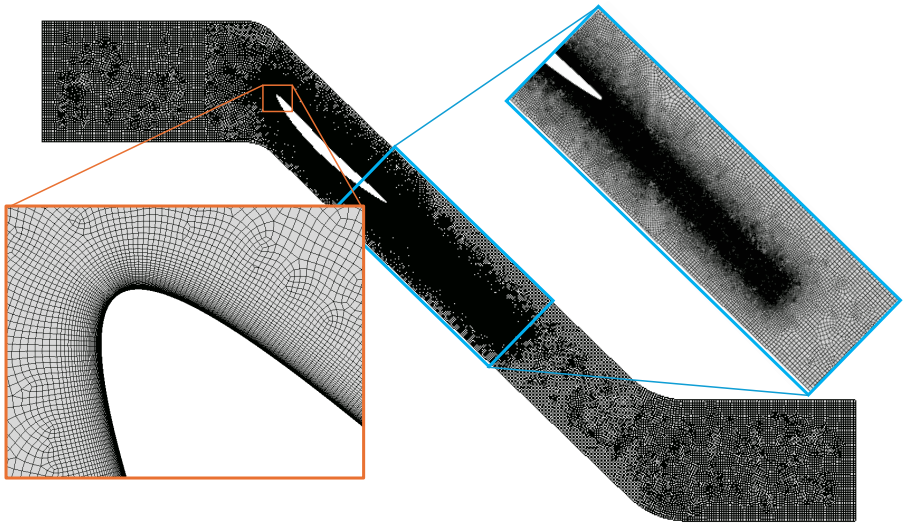


Figure 5 – Computational mesh for CFD analysis

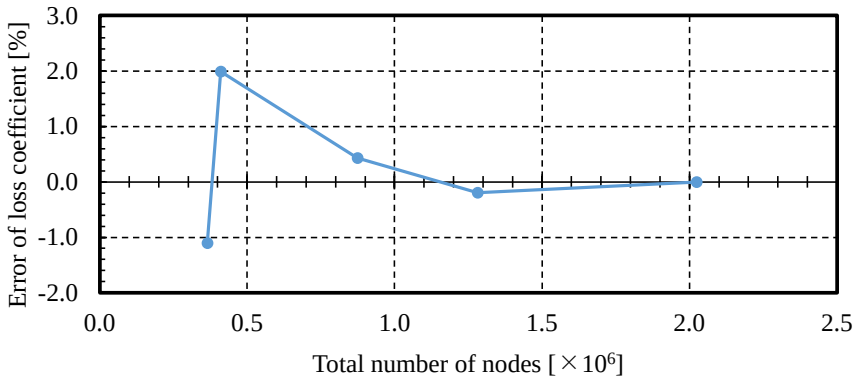


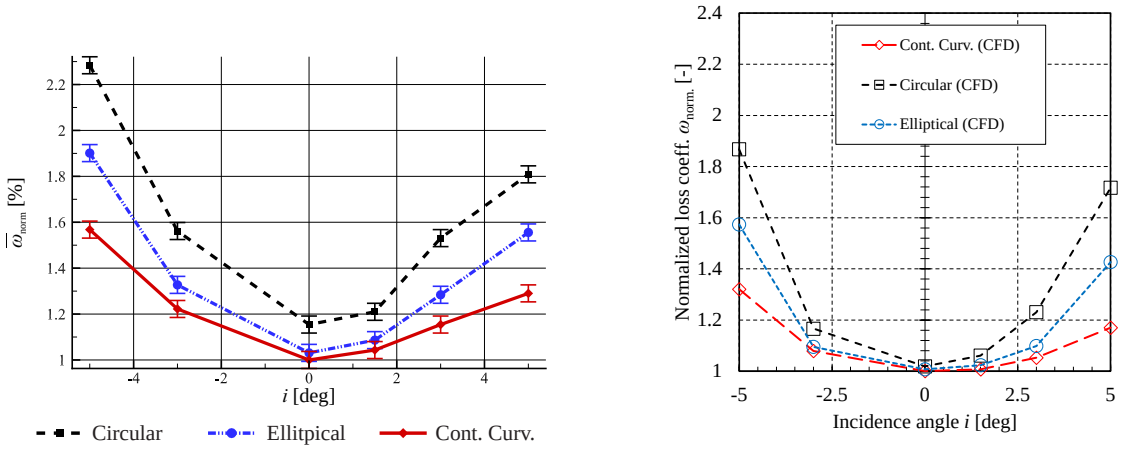
Figure 6 – The result of the grid independence study

Figure 5 shows the computational mesh generated using Ansys Mechanical. The mesh was refined near the wall to capture the boundary layer and wake region. The airfoil boundary layer mesh was constructed to satisfy the condition of $y^+ \simeq 1$. A grid independence study was conducted with five meshes, 'ultra fine', 'fine', 'medium', 'coarse', and 'ultra coarse', in Subsection 3.1.

3. Results and Discussion

3.1 Comparison of Experimental and CFD Results

For the first step, the study of the grid independence is conducted. Five meshes, ultra fine, fine, medium, coarse, and ultra coarse, are generated and the CFD analysis is conducted for each mesh. Each mesh has different number of nodes, 2.02, 1.28, 0.87, 0.41, and 0.36 million nodes, respectively. Figure 6 shows the results of the grid independence study. The horizontal axis is the number of nodes, and the vertical axis is the error of the loss coefficient ω compared to the ultra fine mesh, which is considered as the reference solution. In this grid independence study, the continuous curvature leading edge case at the incidence angle of 0° is used as the test case. From the result, the error of the medium mesh is less than 0.5%, which is considered as acceptable for this study. Therefore, with considering the computational cost, the medium mesh is used for the CFD analysis in this study.
Next, to validate the CFD results, the CFD results and the experimental results are compared. The experimental results are cited from the paper by Lang et al. [6]. Figure 7 shows the comparison of the CFD results and the experimental results. The normalized loss coefficient ω_{norm} is calculated with



(a) Reference results[6]

(b) CFD results

Figure 7 – Comparison of CFD results and experimental results.

the loss coefficient of the continuous curvature leading edge at the incidence angle of 0° $\omega_{\text{cont.curv.,0°}}$.

$$\omega_{\text{norm}} = \frac{\omega}{\omega_{\text{cont.curv.,0°}}}, \tag{5}$$

In Figure 7, for all cases, the CFD results are smaller than the experimental results. This is because the CFD analysis is 2D, while the experiment is 3D.
The experiment of compressor airfoils [6] was conducted in 3D. The distribution of the loss coefficient at the measurement plane in the behind the airfoil shows that the loss coefficient distribution in the spanwise direction is non-uniform, with larger loss coefficients near the wall compared to the mid-span. This non-uniform distribution of the loss coefficient in the spanwise direction cannot be reproduced by 2D CFD analysis, which results in smaller loss values in the CFD results compared to the experimental results.
However, the CFD results can represent the qualitative characteristics of the experimental results. In Figure 7, the experimental and CFD results show that the continuous curvature leading edge has the smallest normalized loss coefficient at all incidence angles, followed by the elliptical leading edge, and the circular leading edge has the largest normalized loss coefficient. The sensitivity to the incidence angle also shows good agreement between the experimental and CFD results. The continuous curvature leading edge has the lowest sensitivity, and the circular leading edge has the highest sensitivity. For each airfoil, the normalized loss coefficient at minus incidence angles is larger than that at plus incidence angles. From these results, the CFD results are qualitatively consistent with the experimental results.

3.2 Performance Variability Due to Geometric Uncertainty

Using the CFD setup described in Subsection 2.2 and the medium mesh, 512 deformed airfoils were randomly generated with Gaussian random distributions for each baseline airfoil by using the PBDMFFD. In this study, as shown in Figure 8, the deformation was applied to the LE region (from 0 to 10% of chord length) of the airfoil, and the PP was set to the LE as a moving point and the 10% chord point as a fixed point. The direction of the deformation was set normal to the airfoil chord line, and the deformation amplitude was defined as the standard deviation of a Gaussian random distribution corresponding to 1° of the metal angle.
Figure 9 shows the distributions of the normalized loss coefficients for three airfoils at the incidence angle of –3°. Because the difference in the loss coefficient between the three airfoils at the incidence angle of 0° is small, as shown in Figure 7, the incidence angle of –3° was selected. In Figure 9, the results reveal that the mean and maximum values of the normalized loss coefficients for circular leading edge are largest, followed by the elliptical leading edge, and the continuous curvature leading edge has the smallest values. On the other hand, the minimum value is approximately the same for

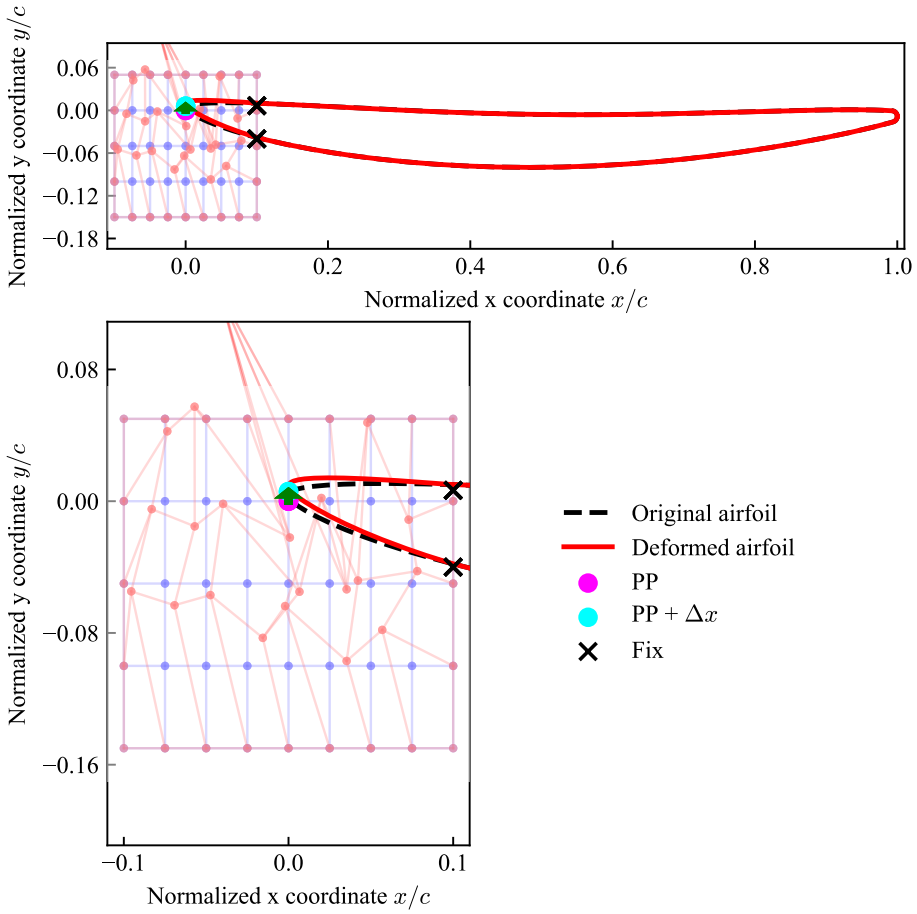


Figure 8 – Setup example of control box and PP for PBDMFFD in this study.

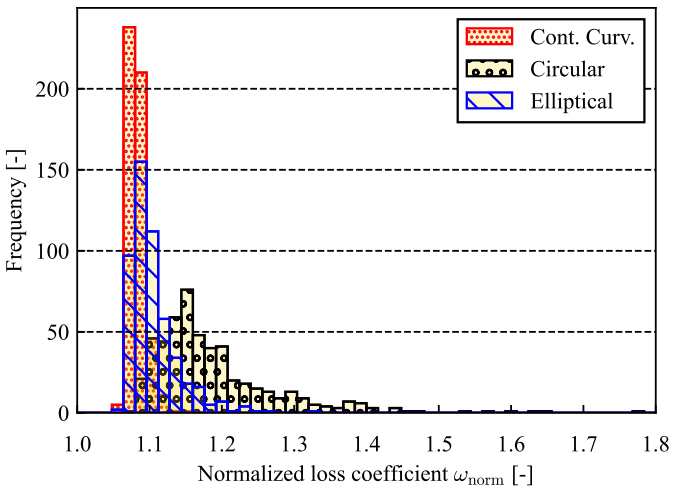


Figure 9 – Normalized loss coefficients of deformed airfoils.

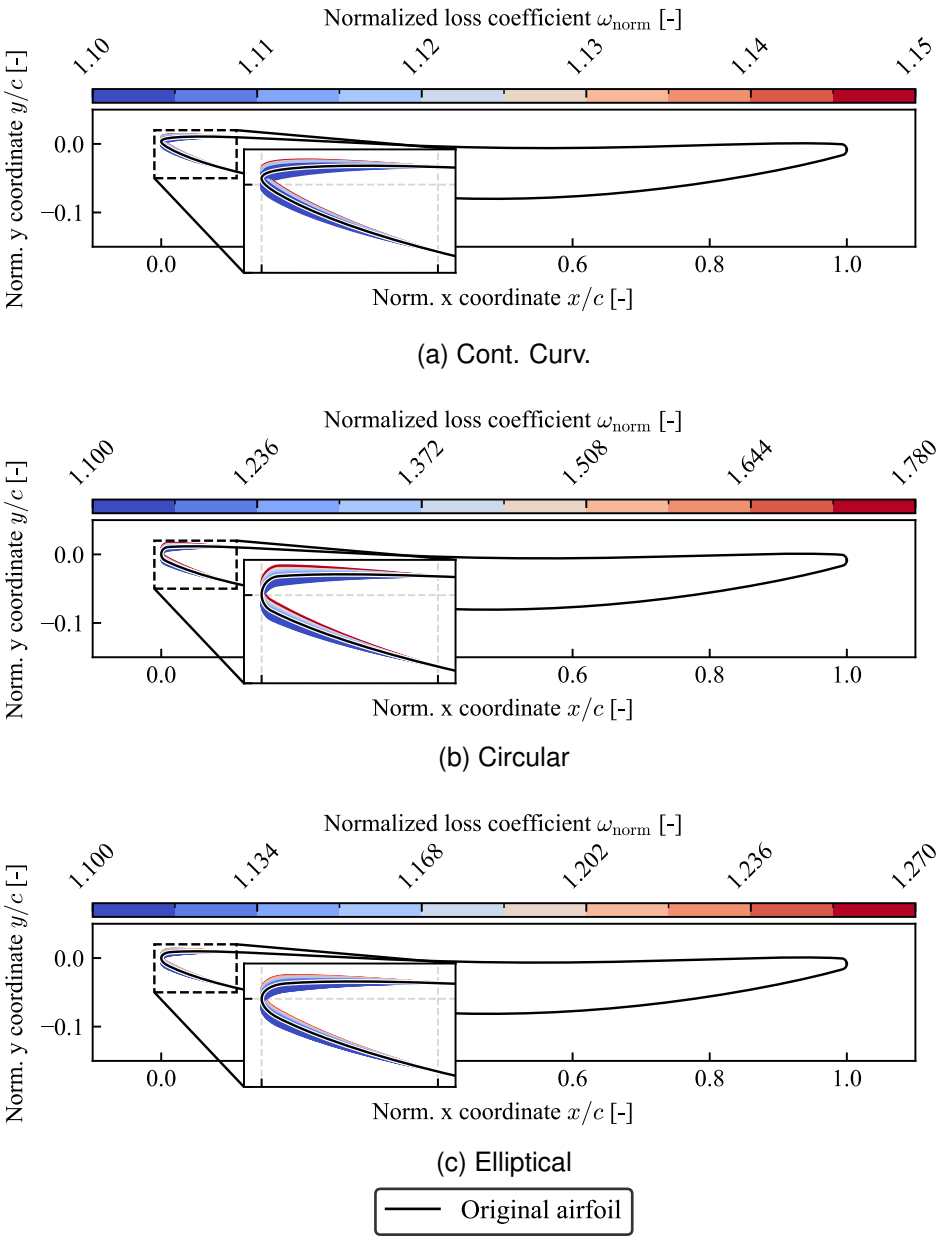


Figure 10 – Loss distribution corresponding to deformation.

all three airfoils. The largest variance is observed in the circular leading edge, followed by the elliptical leading edge, and the continuous curvature leading edge has the smallest variance.

Figure 10 shows the geometries of the deformed airfoils colored according to the normalized loss coefficient ω_{norm} to analyze the relationship between the loss coefficient and the geometry of the airfoil. The black line represents the nominal geometry. Note that the range of the color bar is different for each airfoil. From Figure 10, the distributions of the deformed LE geometries are almost symmetric with respect to the nominal geometry for all three airfoils. On the other hand, the distributions of the normalized loss coefficient corresponding to the deformed geometries are not symmetric with respect to the nominal geometry. The increment of the normalized loss coefficient caused by the deformation of the LE geometry in the 'upper' direction, which is the direction of increasing the metal angle, is larger than the decrement of the normalized loss coefficient caused by the deformation in the 'lower' direction, which is the direction of decreasing the metal angle.

3.2.1 Unsymmetric Behavior of Loss Coefficient with Respect to Deformation Direction

In this study, the deformation was applied using the PBDMFFD method with the Gaussian random distribution. Therefore, the deformation was modeled as an elastic deformation, and the deformed geometries do not exhibit significant deviations from nominal geometry, except near the boundaries of the control box. That is, although the deformation in this study modifies the region near the LE, the change in the LE geometry itself is small. Instead, the primary effect of the deformation is the change in the metal angle caused by variations in the camber near the LE.

The incidence angle is defined by the LE metal angle of the airfoil and the inflow angle of the main flow. Hence, the change in the loss coefficient caused by the variation in the metal angle of the LE can be considered to exhibit a similar trend to that of the loss coefficient variation associated with changes in the incidence angle. As shown in Figure 7, at the incidence angle of around –3°, the nominal airfoils exhibit a large variation in the sensitivity of the loss coefficient to the incidence angle, and the sensitivity tends to increase as the absolute value of the incidence angle becomes larger.

From the above discussion, the variation in the loss coefficient caused by the deformation is attributed to the change in the camber near the LE, which leads to a change in the metal angle. Although the deformation itself is symmetric, the resulting variation in the loss coefficient is asymmetric, which is considered to arise from the fact that the deformation is introduced in a region where the sensitivity of the loss coefficient to the incidence angle varies significantly for the nominal airfoil.

3.2.2 Differences in Maximum Loss Coefficients and Their Variances among Airfoils

To investigate the locations where the loss is generated, the Mach number and entropy distributions for nominal airfoils and deformed airfoils exhibiting the maximum loss coefficient for each airfoil are shown in Figure 11 and Figure 12. The entropy is defined as follows:

$$s = c_p \ln\left(\frac{T}{T_{\mathrm{ref}}}\right) - R \ln\left(\frac{p}{p_{\mathrm{ref}}}\right), \tag{6}$$

where $c_p = 1004.4\,\mathrm{J\,kg^{-1}\,K^{-1}}$ is the specific heat at constant pressure, $R = 287.05\,\mathrm{J\,kg^{-1}\,K^{-1}}$ is the gas constant, T is the temperature, p is the pressure, and $T_{\mathrm{ref}} = 25\,℃$ and $p_{\mathrm{ref}} = 1\,\mathrm{atm}$ are the reference temperature and pressure, respectively. As shown in Figure 11, the entropy distributions indicate that, for all three airfoil configurations, there exists a region near the LE on the pressure-side surface where the entropy becomes extremely large. This region corresponds to a low-Mach number region, as shown in Figure 12. From these results, the increase in the loss coefficient is considered to be caused by flow separation near the LE on the pressure-side surface of the airfoil.

Examining the separation behavior from the Mach number distribution in Figure 12, no significant separation is observed in the region near the LE for the continuous curvature LE airfoil, and a thin boundary layer can be seen developing from the LE. For the elliptical LE airfoil, a slight separation is observed that is not present in the continuous curvature LE, and a thicker boundary layer develops downstream of the separation compared to the continuous curvature LE. For the circular LE airfoil, a larger separation region is observed compared to the elliptical LE, and an even thicker boundary layer develops downstream of the separation compared to the elliptical LE. These difference in the separation behavior can be attributed to the magnitude of the curvature of the LE geometry of the airfoil.

Before mentioned in Subsection 3.2.1, the deformation in this study does not significantly change the LE geometry itself, but rather modifies the region connecting the LE to the region with smaller curvature, which is a common feature among the three airfoils. In the circular LE airfoil, because the magnitude of the curvature in the LE region is small, the acceleration near the LE is relatively mild. However, the difference in curvature between the LE region and the connected region where the curvature is reduced by the deformation becomes large, which is considered to promote flow separation. On the other hand, in the continuous curvature LE airfoil, the magnitude of the curvature in the LE region is large, resulting in a more abrupt acceleration near the LE. However, the nominal geometry is defined such that the curvature is continuously connected, therefore, even if the curvature of the connecting region becomes small due to the deformation, the change in curvature at that region is relatively small. As a result, the flow near the LE follows the geometry, and flow separation is less likely to occur.

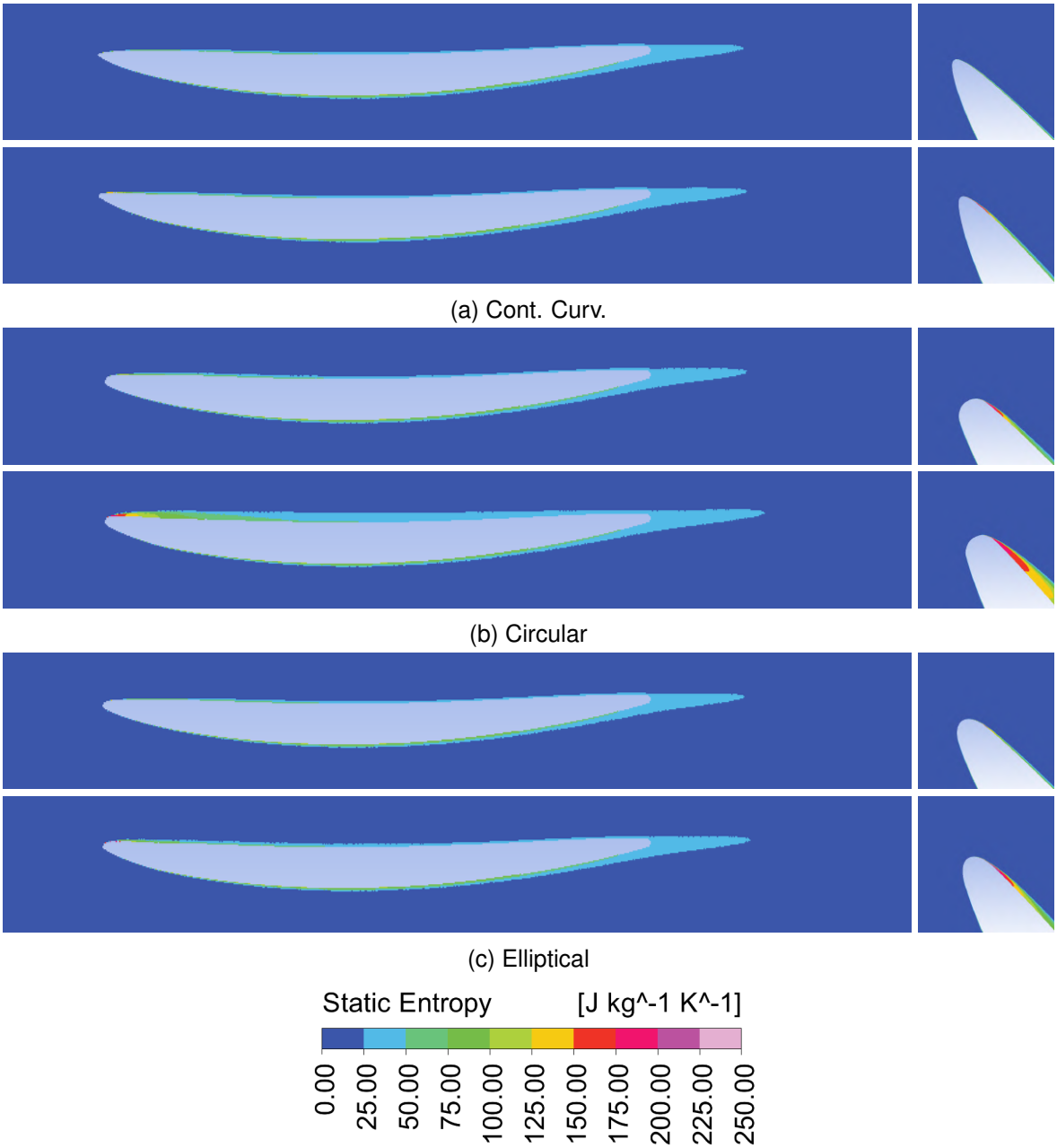


Figure 11 – Entropy distribution of deformed airfoils with maximum loss coefficient. Upper: Nominal; Lower: Maximum.

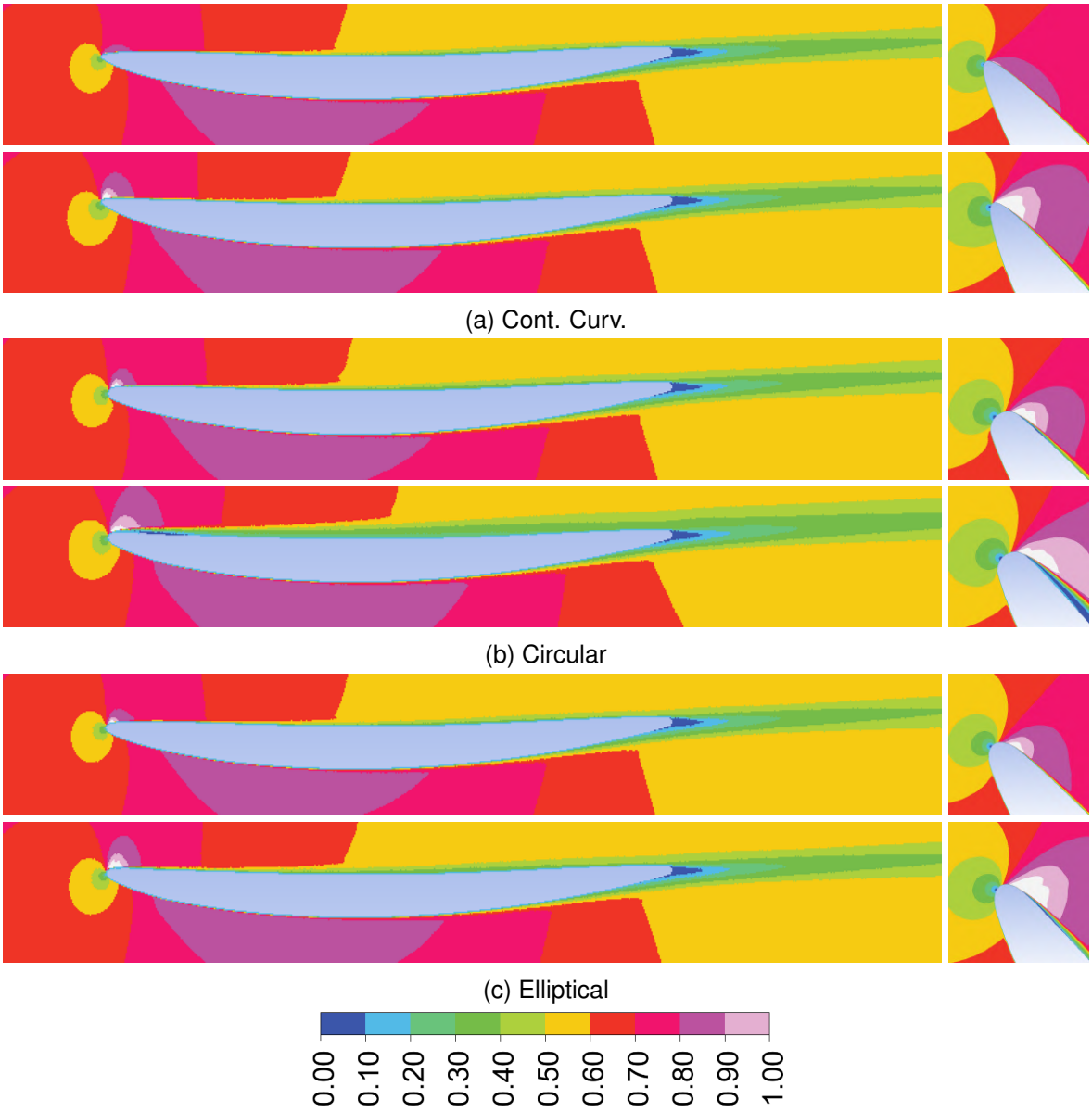
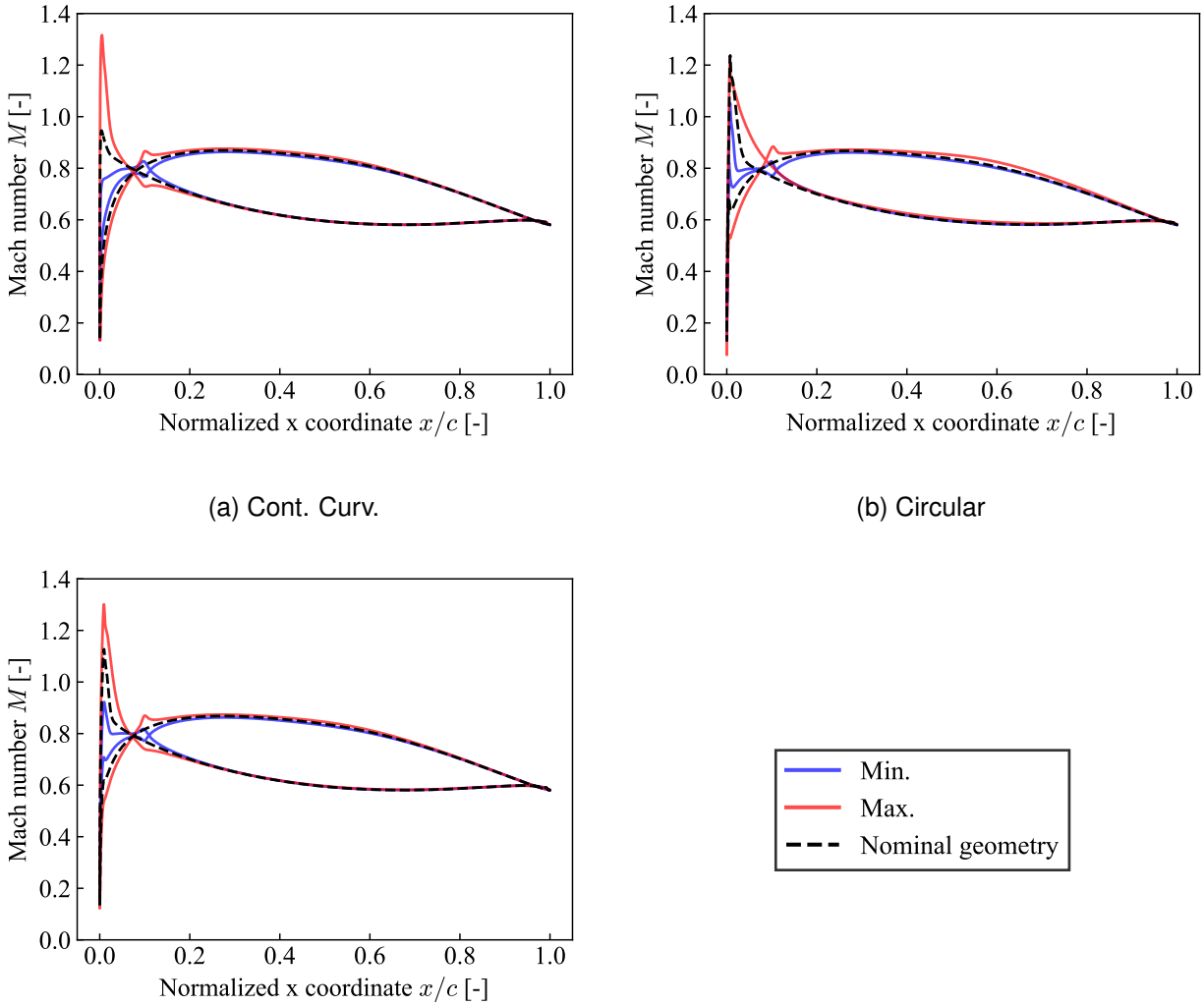


Figure 12 – Mach number distribution of deformed airfoils with maximum loss coefficient. Upper: Nominal; Lower: Maximum.



(a) Cont. Curv.

(b) Circular

(c) Elliptical

Figure 13 – Mach number distribution comparison between deformed airfoils with minimum and maximum loss coefficients.

3.2.3 On the Minimum Achievable Loss Coefficient

To investigate the minimum achievable loss coefficient for each airfoil, the airfoil surface Mach number distributions of the deformed airfoils exhibiting the minimum loss coefficient for each airfoil are shown in Figure 13. From Figure 13, for all three airfoils, the airfoil surface Mach number distributions of the deformed airfoils with the minimum loss coefficient show that the abrupt velocity change near the LE is gentler compared to the nominal geometry. The abrupt velocity change to rapid pressure recovery is one of the main factors contributing to the increase in the loss coefficient, and the deformation to the lower direction, which reduces the metal angle, is considered to mitigate this factor, leading to a decrease in the loss coefficient. On the other hand, the existence of a lower limit for the loss coefficient for all three airfoils in this study can be attributed to the fact that the deformation was applied only in the LE region (from 0 to 10% of chord length). Therefore, a reduction in the loss coefficient due to factors other than the mitigation of the abrupt velocity change near the LE cannot be expected. In fact, for all three airfoils, the flow field and Mach number distribution downstream of the deformation region shows little change, indicating that the deformation primarily affects the flow near the LE, and the flow field downstream of the deformation region remains largely unchanged.

4. Conclusion and Future Work

In this study, the performance variability of three airfoils with different LE geometries was investigated by introducing geometric uncertainties and performing 2D CFD analyses. The CFD results for the nominal airfoils, which were not deformed, showed qualitative agreement with the experimental results, confirming the validity of the CFD analyses in this study. For the deformed airfoils, the distributions of the performance parameters exhibited clear differences among the three airfoils, particularly in terms of the maximum values and variances. The continuous curvature LE airfoil is designed such that the curvature is continuous at the connecting region. Therefore, even if the curvature at the connecting region is reduced by the deformation, the resulting change in curvature remains small. Consequently, compared to with the other airfoils, the flow tend to follow the geometry, suppressing flow separation, which is considered to lead to smaller maximum values and variances in the performance distribution. On the other hand, the circular LE airfoil does not have a continuous curvature at the connecting region. As a result, when the curvature at the connecting region is reduced by the deformation, the change in curvature becomes large, which promotes flow separation. Consequently, the maximum values and variances in the performance distribution are considered to become larger. The elliptical LE airfoil has an intermediate LE geometry between the continuous curvature LE and circular LE airfoils. Therefore, the occurrence of flow separation is not as significant as in the circular LE airfoil, but it is not as suppressed as in the continuous curvature LE airfoil. Consequently, the maximum values and variances in the performance distribution are considered to take intermediate values between those of the continuous curvature LE and circular LE airfoils. The result that significantly different performance distributions are obtained even when similar geometric uncertainties are applied to airfoils with different LE geometries demonstrates the importance of performance evaluation considering geometric variability. Furthermore, these findings are expected to contribute to the development of knowledge for future robust optimal design. In this study, the analyses were performed for only one inflow condition. In the future, analyses for other incidence angles and analyses with different deformation regions will be conducted to gain insights for robust optimal design.

5. Contact Author Email Address

mailto: daisuke.sasaki@omu.ac.jp

6. Copyright Statement

The authors confirm that they, and/or their company or organization, hold copyright on all of the original material included in this paper. The authors also confirm that they have obtained permission, from the copyright holder of any third party material included in this paper, to publish it as part of their paper. The authors confirm that they give permission, or have obtained permission from the copyright holder of this paper, for the publication and distribution of this paper as part of the ICAS proceedings or as individual off-prints from the proceedings.

References

[1] Kato D, Pallot G, Sugihara A, and Aotuka M. Research and development of high performance axial compressor. Technical Report 4, IHI Corporation, 2013.

[2] Motomoli F, editor. *Uncertainty Quantification in Computational Fluid Dynamics and Aircraft Engines*. Springer Cham, 2019.

[3] Yamagami M. Development of compressor aerodynamic technologies for reduction of sfc in aircraft engines. *Journal of Gas Turbine Society of Japan*, 52(6):3–8, 2024.

[4] Omoto K, Sasaki D, Matsui K, and Yamagami M. Numerical simulation study of geometric uncertainty on compressor. In *2025 Asia-Pacific International Symposium on Aerospace Technology*, 2025.

[5] Yamazaki W, Mouton S, and Carrier G. Efficient design optimization by physics-based direct manipulation free-form deformation. In *12th AIAA/ISSMO Multidisciplinary Analysis and Optimization Conference*, 2008.

[6] Lang H, Goto T, Sato D, Kato D, and Jeschke P. Performance analysis of a compressor leading edge without pressure spike at high subsonic speed. *International Journal of Gas Turbine, Propulsion and Power Systems*, 11(4):56–67, 2020.